Title

Inversion recovery UTE based volumetric myelin imaging in human brain using interleaved hybrid encoding

Journal

Magnetic Resonance in Medicine, 83(3)

ISSN

0740-3194

Authors

Jang, Hyungseok
Ma, Yajun
Searleman, Adam C
et al.

Publication Date

2020-03-01

DOI

10.1002/mrm.27986

Peer reviewed

HHS Public Access

Author manuscript

Magn Reson Med. Author manuscript; available in PMC 2021 March 01.

Published in final edited form as:

Magn Reson Med. 2020 March ; 83(3): 950–961. doi:10.1002/mrm.27986.

Inversion Recovery Ultrashort Echo Time (IR-UTE)-Based Volumetric Myelin Imaging in Human Brain Using Interleaved Hybrid Encoding (IHE)

Hyungseok Jang[1], **Yajun Ma**[1], **Adam C Searleman**[1], **Michael Carl**[2], **Jody Corey-Bloom**[3], **Eric Y. Chang**[4,1], **Jiang Du**[1,*]

[1]Department of Radiology, University of California San Diego, San Diego, CA 92103, USA

[2]GE Healthcare, San Diego, CA 92103, USA

[3]Department of Neurosciences, University of California, San Diego, CA 92037, USA

[4]Radiology Service, VA San Diego Healthcare System, San Diego, CA 92037, USA

Abstract

Purpose: Direct myelin imaging can improve characterization of myelin-related diseases such as multiple sclerosis (MS). In this study, we explore a novel method to directly image myelin using inversion recovery prepared hybrid encoding (IR-HE) ultrashort echo time (UTE) MRI.

Methods: The IR-HE sequence uses an adiabatic inversion pulse to suppress the long T2 white matter signal, followed by 3D dual echo HE utilizing both single point imaging (SPI) and radial frequency encoding, where the subtraction image between two echoes reveals the myelin signal with high contrast. To reduce scan time, it is common to obtain multiple spokes per IR. Here, we invented a novel method to improve the HE, adapted for the multi-spoke IR imaging— termed interleaved HE (IHE)—where SPI encoding is interleaved between radial frequency encodings near nulling point to allow more efficient IR-signal suppression. To evaluate the proposed approach, a computer simulation, a myelin phantom experiment, an *ex vivo* experiment with a cadaveric MS brain, and an *in vivo* experiment with 8 healthy volunteers and 13 MS patients were performed.

Result: The computer simulation showed that IR-IHE allows for improved contrast of myelin signal with reduced imaging artifacts. The myelin phantom experiment showed IR-IHE allows direct imaging of myelin lipid with excellent suppression of water signal. In the *ex vivo* and *in vivo* experiments, the proposed method demonstrated highly specific imaging of myelin in white matter of the brain.

Conclusion: IR-IHE allows for time-efficient, high contrast direct myelin imaging and can detect demyelinated lesions in MS patients.

Keywords

UTE; Hybrid Encoding; Inversion Recovery; Myelin; Multiple Sclerosis

[*]Corresponding Author: Jiang Du, Ph.D., jiangdu@ucsd.edu, University of California, San Diego, Department of Radiology, 200 West Arbor Drive, San Diego, CA 92103-8226, Phone (619) 471-0519 | Fax (619) 471-0503.

Introduction

Demyelination is commonly associated with several neurological diseases in the central and peripheral nervous systems such as multiple sclerosis (MS), mild traumatic brain injury (mTBI), acute disseminated encephalomyelitis, and central pontine myelinolysis. Among them, MS is the most common immune-mediated demyelinating inflammatory disease, afflicting nearly one million people in the USA and over 2.3 million people globally (1,2). MS is characterized by multiple foci of demyelination in the brain or spinal cord that are disseminated in time and space, which can result in debilitating visual, motor, sensory, and autonomic problems (3). Improved detection and characterization of these demyelinated lesions is essential to improving the diagnosis of the demyelinating diseases and evaluation of treatment response.

Magnetic resonance imaging (MRI) is the gold standard non-invasive imaging modality to identify demyelination and remyelination. Clinically, T2-weighted imaging is commonly used for the characterization of lesions, with fluid-attenuated inversion recovery (FLAIR) and fast spin echo sequences (4,5). However, these sequences are not specific for myelin and can be challenging to interpret. Many advanced MRI techniques have shown some utility in detecting and characterizing demyelinated lesions, including magnetization transfer, diffusion-weighted imaging, and susceptibility-weighted imaging (4,6).

Direct imaging of myelin lipid protons could provide highly specific information to characterize demyelinating lesions in morphological and quantitative ways, which may allow for improved diagnosis and assessment of prognosis in the demyelinating diseases. Unfortunately, it is challenging to directly image myelin protons in white matter using MRI due to the low MR signal resultant from relatively low myelin proton density and from rapid signal decay (T2* less than 0.5 ms at 3T) (7,8). A breakthrough development demonstrated that direct myelin imaging is feasible using inversion recovery (IR) preparation followed by ultrashort echo time (UTE) MRI, allowing direct capture of the rapidly-decaying myelin signal with greatly improved dynamic range (9–12). The following strategies are applied: First, an adiabatic IR pulse preparation is applied to provide robust suppression of signals from the long T2 components in white matter, which are mainly water. Second, dual echo UTE imaging is used to suppress the remaining long T2 gray matter signal and residual long T2 white matter signal by subtracting the second echo from the first one. Since the main short T2 tissue in white matter is myelin, the remaining signal reflects myelin content (7–11,13,14). In practice, for 3D IR-UTE to achieve a clinically feasible scan time, multiple spokes (typically over ~10) are consecutively acquired after each IR preparation (multi-spoke IR). The disadvantage of multi-spoke IR imaging is the inclusion of data acquired at suboptimal TIs, which can degrade long T2 white matter suppression.

Hybrid encoding (HE), such as Pointwise Encoding Time Reduction With Radial Acquisition (PETRA) (15), was first proposed to acquire the missing central k-space data due to RF coil deadtime by utilizing single point imaging (SPI) encoding (16). A generalization of PETRA, called ramped hybrid encoding (RHE) (17), has also been proposed to allow more flexible and efficient encoding and to resolve the unwanted slice

selectivity problem (18). More active and aggressive utilization of SPI in HE has also been demonstrated in the literature to allow high temporal resolution or improve image quality (19).

In this study, we explore the efficacy of IR prepared HE (IR-HE) for direct morphological volumetric myelin imaging, where the IR prepared dual echo 3D HE is performed with a multi-spoke acquisition scheme. To further improve image contrast for myelin and to reduce scan time, a novel encoding scheme is presented, termed interleaved HE (IHE), where SPI encoding is interleaved with radial encoding near the optimal TI of the multi-spoke IR acquisition. This strategy allows for the SPI-encoded central region of k-space, which largely determines image contrast, to be acquired near the optimal TI for white matter suppression, allowing acquisition of a large number of spokes per IR. The proposed framework is evaluated by computer simulation, myelin phantom experiments, *ex vivo* qualitative imaging of a cadaveric MS brain, and *in vivo* qualitative imaging of healthy volunteers and MS patients.

Methods

Inversion Recovery Dual Echo Hybrid Encoding

In this study, UTE imaging is utilized to directly resolve the myelin signal, which has an extremely short T2* (<0.5 ms at 3T) (7,8). In UTE imaging, echo subtraction has been widely used to obtain high contrast for short T2* tissues, such as tendon and ligament, with long T2 component suppressed (20,21). Similarly, to suppress other tissues and to enhance the myelin contrast, dual echo UTE imaging can be performed, where a UTE image and a second gradient recalled echo image are obtained in a single acquisition. When the second echo is obtained soon after the myelin signal decays to near zero, it is theoretically possible to distinguish the myelin signal from other tissues by subtracting the second echo from the UTE, thus suppressing the longer T2 signals from white matter, gray matter, and CSF. Unfortunately, the MR signal from the myelin is low due to the relatively low proton density and short T2* decay (7,8); therefore, the myelin signal can be contaminated by noise, aliasing/streaking artifacts from the surrounding tissues (long T2 white matter or gray matter), and low frequency signal bias due to B1 inhomogeneity or reconstruction error (e.g., uncorrected readout delay, eddy current effect, imperfection in gridding process), which can significantly impair the myelin signal. Moreover, severe discretization errors can be introduced during the analog-to-digital conversion due to the limited dynamic range of current MR systems if the receiver gain is adjusted to the long T2 white matter or gray matter signal in pre-scan, which can be exacerbated in the echo subtraction.

To address the abovementioned issues, IR preparation is incorporated into the dual echo UTE imaging, where the long T2 signals from white matter are selectively and robustly suppressed, as demonstrated in our previous work on 2D UTE (9–11) and by others (22). The IR-based imaging has been utilized to achieve high T1 contrast or tissue suppression (7,23–27). Figure 1–a illustrates the typical T1 recovery curves of gray matter, white matter, and myelin after application of the adiabatic inversion pulse. By carefully selecting inversion time (TI) matched to the nulling point of the white matter, the signal from white matter can be suppressed. Due to the extremely short T2* of myelin (<0.5 ms) and relatively long

duration of the adiabatic inversion pulse (~8 ms), the myelin is not inverted, but partially saturated (28). Once the white matter signal is suppressed by IR, the remaining signal from gray matter and CSF (T1 longer than white matter) is suppressed by utilizing the subsequent dual echo hybrid encoded UTE imaging. Note that multiple spokes are acquired after each IR preparation to reduce the scan time, centered on the optimal TI, as shown in Figure 1–b. This study used the GE-provided adiabatic inversion pulse (Silber Hoult pulse, pulse width = 8.64 ms).

In the dual echo HE, two images at UTE and later echo (TE2) are acquired in a single acquisition, as shown in Figure 1–c (17). In the HE, gradients are applied before RF coil deadtime to optimize encoding time and, due to the deadtime (blind time during RF transmit/receive switching), the missing k-space is filled by utilizing SPI. In this study, zero gradient excitation-based hybrid encoding is employed, as in (19,29,30), to allow slab selection to reduce aliasing/streaking artifacts (19), utilizing a Shinnar–Le Roux pulse (pulse width = 1132 μs, bandwidth = 16kHz) with minimum phase, iso-delay, and variable-rate selective excitation (VERSE) specially designed for UTE imaging. Figure 1–d illustrates an example of the hybrid encoded sampling pattern, where both Cartesian SPI and radial frequency encoding are utilized to acquire k-space data. Note that it is possible in HE to reconstruct the image with different k-space subregion (low resolution part) by selecting different TEs, as demonstrated in (19). In this study, the relative radius of the spherical k-space subregion encoded by SPI, R_{SPI}, was defined by the ratio of the maximum k-space coordinate in SPI-encoded region to the maximum coordinate in entire k-space as shown in the following equation:

$$R_{SPI}(TE) = \frac{\gamma}{k_{max}} \int_0^{TE} G(\tau) d\tau, \quad (1)$$

where γ is a gyromagnetic ratio of proton, G is a shape of gradient waveform, and k_{max} is the maximum k-space coordinate.

Interleaved Hybrid Encoding

In IR-prepared 3D UTE imaging, it is essential to acquire multiple spokes after each IR preparation for time-efficient data acquisition, as shown in Figure 1–b, which is a common approach to reduce the additional scan time imposed by long signal preparation (31,32). Unfortunately, there is a trade-off in this approach, as the image contrast is inevitably degraded due to the spokes acquired at suboptimal TIs for white matter suppression. To address this issue, we propose a strategy of interleaving SPI encodings between radial frequency encodings.

In conventional hybrid encoding techniques such as PETRA and RHE, the radial frequency encoding and the SPI encoding are performed separately, one after the other, as illustrated in Figure 2–a. However, this approach is not suitable for multi-spoke IR imaging, since the central k-space encoded by SPI, which significantly contributes to the image contrast, is contaminated by the suboptimal TIs. The proposed IR-prepared IHE (IR-IHE) addresses this by interleaving SPI encodings to the time slot near the optimal TI, as shown in Figure 2–b, so that the data in the central region of the k-space are acquired with the best TIs. Thus, IR-

IHE allows for more efficient suppression of the long T2 white matter signal with a high degree of multi-spoking for IR-prepared imaging.

Computer Simulation

To verify the efficacy of IR-IHE, a computer simulation was performed. First, a 2D high resolution digital head phantom (654×654) comprised of six components (CSF, gray matter, white matter, myelin in white matter, skull bone, and subcutaneous fat) was generated, as shown in Figure 3–a. To generate a head segmentation map, an exemplary brain map provided by an open-source brain segmentation tool (MICO: http://www.imagecomputing.org/~cmli/) was used, which provided labeling for white matter and gray matter. The three additional segments (CSF, skull, and skin fat) were manually added. Four foci of demyelination comprised of white matter and CSF were additionally generated on the white matter to simulate a MS brain.

Based on the generated head segmentation map, Bloch simulation was performed with the following T1 and T2* model at 3T: T1/T2* = 4000/100 ms for CSF, 1500/100 ms for gray matter, 1000/50 ms for white matter, 350/0.3 ms for myelin, 220/0.3 ms for skull bone, and 400/20 ms for subcutaneous fat. For simplicity, proton density (PD) was set the same for all components, except for myelin and skull bone, which had PDs set to 10% of the other components. The multi-spoke IR-UTE imaging was simulated, including IR-HE, IR-IHE, and IR-pure radial UTE (IR-PRUTE), where each group of multi-spokes was centered at the desired nulling point of the white matter.

For the simulation of the IR-HE and IR-IHE, the following imaging parameters were simulated: flip angle (FA) = 15°; readout bandwidth±125 kHz; maximum gradient amplitude (Gmax) = 26.4 mT/m; gradient slewrate = 120 mT/m/ms; field of view (FOV) = 220×220 mm^2; TR/TI = 1000/379.9 ms; TE = 0.07/1.87 ms; Tau (spoke-to-spoke timing) = 6 ms; matrix size = 220×220; 773 spokes (81 SPI+692 radial). IR-PRUTE was simulated with matched parameters, but omitted SPI encoding. All radial spokes in IR-HE, IR-IHE, and IR-PRUTE were reordered using bit-reversal permutation scheme for pseudo-randomization to alleviate streaking artifacts caused by inter-spoke signal variation, which was easily performed by reversing an index in binary number (33). For example, the spoke index 10 (1010 in binary number) was re-assigned as 5 (0101 in binary number after reversal). The simulation was repeated with 7 different levels of multi-spoking (1, 11, 21, 31, 41, 51, and 61 spokes per IR). Moreover, an expanded simulation was performed with 4 different Taus (3, 6, 9, and 12ms) and 4 different myelin proton densities (0, 5, 10, and 15%).

The simulation was performed using Matlab 2017b (The Mathworks Inc, Natick, MA, USA). The k-space data from the brain image simulated at the given TI and encoding time for each k-space sampling coordinate was sampled using Non-uniform FFT (NuFFT) (34)-based inverse gridding. Gaussian noise with a standard deviation matched to 0.6% of the proton density of gray matter was added to the sampled data.

Myelin Phantom

For the phantom study, H_2O-myelin and D_2O-myelin phantoms were prepared by compounding myelin lipid powder (type 1 bovine brain lipid extract, Sigma-Aldrich B1502,

St. Louis, MO) with distilled, deionized H_2O or D_2O in 1.0 mL syringes. The myelin lipid powder had been previously prepared in D_2O, then lyophilized to reduce residual water and solvent contamination. The phantoms were prepared at 15% weight/volume (15 grams of solute per 100 mL of solution) in order to approximate the physiological concentration of myelin in white matter.

Imaging was performed with a 3T clinical MR system (MR750, GE Healthcare, Waukesha, WI, USA). The H_2O-myelin phantom was imaged using IR-IHE to suppress water signal, while the D_2O-myelin phantom was imaged using regular HE without IR preparation. Note that D_2O signal is not visible in the regular MRI and, therefore, the myelin in the D_2O-myelin phantom can be directly imaged without IR. A custom-made transmit/receive birdcage RF coil was used for imaging. For the H_2O-myelin phantom, the following imaging parameters were used: FA = 10°; FOV = 40×40×20 mm^3; matrix size = 128×128×20; readout bandwidth = ±250 kHz; Gmax = 45 mT/m; gradient slewrate = 160 mT/m/msec; TR = 1000 ms; TI = 260, 300, 320, 335, 350, 370, or 400 ms; Tau = 11 ms; TE = 0.06/2.46 ms; 6343 spokes (491 SPI + 5852 radial in bit-reverse order); 10 spokes acquired per IR; and scan time per acquisition = 10 min 34 sec. Once the best TI was found empirically, three additional scans (1 dual echo and 2 single echo acquisitions) were performed for T2* fitting with the best TI of 335 ms and TE = 0.06/2.46 ms (dual echo scan), 0.2 ms (single echo scan), or 0.4 ms (single echo scan). The D_2O-myelin phantom was imaged with the same parameters as above except for the following parameters: TR = 80 ms, 4787 spokes (491 SPI +4296 radial), no IR, and scan time per acquisition = 6 min 24 sec.

Cadaveric MS Brain

To evaluate IR-IHE in the human brain, an *ex vivo* experiment was performed with a cadaveric MS brain specimen (45-year-old male). The brain was imaged in a clinical 3T MR system (MR750, GE Healthcare) with the following imaging parameters in accordance with IRB-approved protocols: GE 8-ch receive-only head coil; FA = 10°; FOV = 240×240×180 mm^3; matrix size = 240×240×45; readout bandwidth = ±250 kHz; Gmax = 40 mT/m; gradient slewrate = 150 mT/m/msec; TR/TI = 500 ms/155 ms; TE = 0.06/1.30 ms; Tau = 5ms; 68033 spokes (1371 SPI + 66662 radial in bit-reverse order); 20 spokes acquired per IR; and scan time per acquisition = 28 min 56 sec. Two additional single echo scans were performed with TE = 0.26 or 0.66 ms for T2* estimation with other parameters matched.

In vivo Experiment

An *in vivo* experiment was performed with 8 healthy volunteers (3 females and 5 males) with a median age of 35 years (range, 25–56 years) and 13 MS patients (9 females and 4 males) with a median age of 51 years (range, 38–69 years) using a clinical 3T MR system (MR750) in accordance with IRB-approved protocols, using the following imaging parameters: GE 12-ch receive-only HNU coil; FA = 10°; FOV = 220×220×151 mm^3; matrix size = 220×220×42; readout bandwidth = ±250 kHz; Gmax = 33 mT/m; gradient slewrate = 120 mT/m/msec; TR/TI = 1000 ms/320 ms; TE = 0.07/1.87 ms; Tau = 6ms; 24529 spokes (901 SPI + 23628 radial in bit-reverse order); 60 spokes acquired per IR; and scan time = 6 min 50 sec.

Clinical Sequences

For the MS brain and the MS patients, clinical sequences, namely, magnetization prepared rapid acquisition with gradient echo (MP-RAGE) (35) and FLAIR, were added to the experiment for comparison. The imaging parameters for MP-RAGE were as follows: FA = 12°; FOV = 256×256×178 mm^3; matrix size = 256×256×148; readout bandwidth = ±41.7 kHz; TE = 3.2 ms, TR/TI = 8.2/450 ms; acceleration factor = 4; scan time = 5min. The imaging parameters for FLAIR were as follows: FA = 90°; FOV = 256×256×256 mm^3; matrix size = 256×256×256; readout bandwidth = ±41.7 kHz; TE = 116.5 ms, TR/TI = 7600 ms/2162 ms; acceleration factor = 4; scan time = 6min 54sec. MP-RAGE was performed in axial slice direction, while FLAIR was performed in sagittal slice direction and reformatted to axial in post-processing.

Image Reconstruction and Data Analysis

The codes for image reconstruction and data analysis were written in Matlab 2017b (The Mathworks Inc. Natick, MA, USA) and executed offline. The sampled k-space data in the computer simulation and in the *ex vivo* and *in vivo* experiments were reconstructed using NuFFT (34) with 2x oversampling rate and a kernel width of 5 pixels. Iterative density compensation was performed to estimate the density function at each k-space point and used for reconstruction (36). The k-space data obtained with a healthy volunteer were reconstructed at four different TEs (32, 52, 62 and 70μs) with four different R_{SPI} (0.007, 0.016, 0.023, and 0.030).

Quantitative evaluation of T2* was performed on each phantom and specimen. T2* values were obtained using a Levenberg-Marquardt fitting algorithm based on a single-component model. Contrast-to-noise ratio (CNR) measurements were performed to evaluate the different imaging techniques in the computer simulation and in the *in vivo* experiment with a healthy volunteer. The CNR between myelin and the surrounding tissue was calculated as their signal difference divided by background noise. In the computer simulation, CNR was calculated between global white matter/myelin segment and gray matter segment. In the *in vivo* experiment, the CNRs were calculated by repeating the measurement four times in the local ROIs near the left-posterior part of the brain.

Results

Computer Simulation

Figure 3–b shows the result of the multi-spoke IR imaging simulated at the nulling point of white matter with 1, 11, 21, 31, 41, 51, or 61 spokes per IR, using the IR-PRUTE, IR-HE (i.e., with conventional sequential sampling scheme), or IR-IHE. As shown in the figure, at a high number of spokes per IR, signal intensity and contrast of myelin in the IR-PRUTE and IR-HE notably deviate from the reference standard (1-spoke per IR), while the IR-IHE exhibits much improved myelin images with less imaging artifacts. In Supporting Information Figure S1–a, IR-IHE shows consistently accurate lesion detection, depicting similar morphology of lesions compared to the reference standard, while IR-PRUTE and IR-HE show the lesions deviated from the reference standard (1-spoke per IR) in its shape and intensity at a high number of multi-spokes.

Note that a strong, low frequency artifact is introduced in IR-HE due to the SPI sampled with different image contrasts, causing inter-sample signal variation and, thus, modulating the central region of the k-space at a high degree of multi-spoking. In IR-PRUTE, streaking artifact is visible due to the inter-spoke signal variation, which is not fully addressed by randomization of spokes at a high degree of multi-spoking. Supporting Information Figure S1–b shows root mean square error (RMSE) of myelin signal calculated with respect to the reference standard and CNR calculated between myelin and gray matter with different numbers of spokes per IR, where IR-IHE shows overall better performance in RMSE and CNR as compared to the IR-PRUTE and IR-HE. IR-HE shows steeply decreasing CNR over the number of spokes per IR due to the low frequency artifact.

The results with the expanded simulations with different Taus and myelin densities can be found in Supporting Information Figure S2 and S3, respectively.

Myelin Phantom Experiment

Figure 4–a shows the H_2O-myelin phantom imaged with IR-IHE at different TIs, demonstrating robust suppression of the long T2 component (i.e., water) with TI = 335 ms. The imaging was repeated at different TEs at the empirically determined best TI of 335 ms. As can be seen in Figure 4–b, the estimated T2* with IR-IHE was 222.3±4.1 μs, which was consistent with the results in our previous study (150–400 μs) (8,10). The D_2O-myelin phantom was imaged at four different TEs with HE without IR preparation, where the estimated T2* was 362.5±18.8 μs, which showed elevated T2* over that of the H_2O-myelin phantom, presumably due to residual water in the D_2O-myelin phantom.

Cadaveric MS Brain Experiment

Figure 5–a shows a morphological myelin image obtained with a cadaveric MS brain using the proposed IR-IHE, as well as the corresponding clinical images (MP-RAGE and FLAIR), where the demyelinated lesions are clearly indicated with yellow arrows in the subtraction image in IR-IHE. Figure 5–b shows the estimated T2* fitting of the averaged signal in the yellow ROI in Figure 5–a, with estimated T2* of 271.8±2.6 μs. This estimated T2* value was very similar to the T2* value estimated with cadaveric human brains in our previous study (~200–350 μs) (10). As depicted, the subtraction image clearly delineates the morphology of demyelinated MS lesions.

In vivo Experiment

For all 8 healthy subjects, the proposed IR-IHE was able to suppress white matter signal and to clearly visualize the remaining myelin lipid signal in subtraction images. Figure 6–a shows the UTE, the second echo (TE2), and the resultant myelin image (the subtraction image between the UTE and the second echo) from a healthy volunteer (30-year-old male), obtained using IR-HE or IR-IHE. As shown in the zoomed-in view, the strategy of interleaving SPI in the IR-IHE dramatically improves the myelin contrast, which is expected based on the computer simulation results. The measured CNR between myelin and the surrounding tissues in the myelin image was 2.3±0.6 in the IR-HE and 4.8±0.7 in the IR-IHE. Figure 6–b shows four different myelin images reconstructed using the same dataset obtained by the IR-IHE, with different R_{SPI}. As shown in the figure, the background signal

(mostly from the remaining gray matter) tends to be spatially biased with the smaller R_{SPI}. For example, the gray matter in the back of the brain is shown more brightly than in the anterior region of the brain, which is probably due to eddy currents and imperfect reconstruction causing low frequency error in central k-space. As shown by the green arrows, such signal bias is well-suppressed with larger R_{SPI}, since SPI is robust to eddy current-induced errors (19). The measured CNR between myelin and the surrounding tissues was 3.5±0.8, 3.9±0.7, 4.1±0.7, and 4.8±0.7 for IR-IHE with R_{SPI} = 0.007, 0.016, 0.023, and 0.030, respectively.

For all 13 MS patients, the IR-IHE was able to detect demyelinated lesions in white matter in subtraction images. Figure 7 shows the IR-IHE images and the corresponding clinical MR images (MP-RAGE and FLAIR) obtained with two representative MS patients (Patient A: 59-year-old female, Patient B: 51-year-old female). The demyelinated areas can be detected by the proposed IR-IHE imaging as regions where there is loss of the normal myelin signal (red arrows).

Discussion

This study demonstrated that direct qualitative imaging of myelin protons is achievable on a clinical 3T scanner using the proposed multi-spoke IR-IHE. In the myelin phantom experiment, we showed that the T2* of myelin is around 200–350μs, which can be imaged using IR-IHE. The T2* of myelin measured in the *ex vivo* experiment was also within range. In the computer simulation, we showed that the proposed IR-IHE method allows better white matter suppression that is robust to the degradation of image contrast due to multi-spoking as compared to conventional imaging schemes. This was verified in the *in vivo* experiments, where we showed the efficacy of interleaving SPI with radial encoding in IR-IHE so that the SPI, and thus central k-space, were acquired near the optimal TIs. Additionally, we showed that IR-IHE was able to detect demyelinated lesions in a cadaveric MS brain and *in vivo* in MS patients. Compared with clinical MR sequences, the myelin images generated with the IR-IHE are more specific and should provide better morphologic characterization of demyelinated lesions.

For 3D IR-UTE-based myelin imaging, where a long TR is essential to improve SNR, the strategy of acquiring one spoke per IR is not feasible due to the long scan time; therefore, a multi-spoke acquisition scheme is essential to achieve a clinically acceptable scan time (<10 min). In the *in vivo* experiments of this study, the TR was set to 1 sec to secure a reasonable SNR for myelin. The proposed IR-IHE scheme with the strategy of interleaving SPI near the optimal TI allows utilization of a high degree of multi-spoking for IR imaging (e.g., 60 spokes acquired per IR preparation in the *in vivo* protocol), achieving both good image contrast with white matter suppressed near-completely and a clinically feasible scan time of less than 7 min. If only one spoke was acquired per IR, the scan time would be 7 hours.

In the computer simulation demonstrated in Figure 3, the IR-IHE shows dramatically suppressed imaging artifacts over the IR-PRUTE and IR-HE. As shown, the IR-HE introduces a strong, low frequency artifact in the cases with multi-spoke IR. This is due to the inconsistent signal weighting in SPI samples in the central k-space (the low resolution

part). In radial sampling, this issue is also present, introducing streaking-like artifact with a high degree of multi-spoke acquisition. However, the streaking artifact is less coherent than SPI (i.e., 3D pure phase encoding) and can be suppressed relatively easily by randomizing the order of spokes, which is commonly used in undersampled radial MR acquisitions (33,37,38). In this study, we utilized the bit-reversal pseudo-randomization for the radial sampling part in order to make the streaking artifact more incoherent.

The IR-IHE technique utilizing interleaved SPI encoding and randomized radial encoding addresses the abovementioned artifacts which manifest in a multi-spoke IR scheme. Note that in the computer simulation shown in Figure 3–b, the proposed method does not exhibit this low frequency artifact due to nearly-consistent IR contrast in SPI samples (always acquired near TI, the nulling point of white matter). The efficacy of the IR-IHE is also demonstrated in the results of the *in vivo* experiments. Figure 6–a shows that the image contrast is dramatically improved by applying the proposed interleaving strategy as compared to the conventional HE which sequentially performing radial frequency and SPI encoding. Figure 6–b shows that a larger SPI covering of the central region of k-space allows for better myelin contrast, presumably owing to the robustness of SPI to eddy current effects (19).

Another advantage of IR-IHE for myelin imaging is shorter effective TE due to SPI, which allows one to apply the gradient before RF coil deadtime. In HE, a certain extent of the central region in k-space (e.g., R_{SPI}=0.030 in the *in vivo* experiment), which most significantly contributes to the signal intensity and image contrast, is encoded at a constant TE (at a nominal TE) by SPI. Therefore, the resultant image more accurately reflects the actual signal at the nominal TE compared to conventional UTE imaging in which the central region in k-space is composed of the data sampled at different TEs, equal to or longer than the nominal TE (thus, delayed effective TE). Therefore, HE can be advantageous for imaging tissues with extremely short T2*, such as myelin and bone. Note that in the computer simulation (Supporting Information Figure S1–b), IR-PRUTE shows overall lower CNR than IR-HE and IR-IHE, presumably due to the delayed effective TE. The benefit of shorter encoding time (readout duration) in HE has been reported in the literature, which reduces short T2* blurriness effect and chemical shift artifacts (15,17). However, the influence of effective TE in different UTE techniques still needs to be rigorously investigated for imaging extremely short T2* contents such as myelin, which we will explore in future studies.

The key idea of IR-IHE can be generalized to improve multi-spoke IR imaging combined with other encoding schemes. The key concept is to determine the best way to divide k-space into subsections and allocate the best time slots near the optimal TI to the sub-regions which most significantly contribute to image quality. Note that the HE inherently has two subsections in k-space (namely, central k-space encoded by SPI and outer k-space encoded by frequency encoding), so we were able to interleave SPI encodings near the optimal TI to improve image contrast. Likewise, k-space can be subdivided by performing the segmented radial frequency encoding with the different readout bandwidths as in Water- and Fat-suppressed Proton Projection MRI (WASPI) (39). In that case, the best TI can be assigned to the spokes in the central k-space, which will require shorter scan time than the HE-based

method. However, other benefits of SPI encoding (e.g., robustness to eddy currents) will be lost.

Although a larger SPI region in k-space improves image quality, as demonstrated in Figure 6–b, it is difficult to freely control the R_{SPI} for the following reasons: First, the R_{SPI} depends on the shape of the gradient waveform. For example, if stronger gradients are applied, the SPI-sampled points in the k-space will spread faster and the R_{SPI} will become larger at any given TE. Second, a larger SPI region requires more SPI-encoding points (or higher sampling density) to avoid the fold-over artifact (or aliasing) exhibited in x, y, and z directions due to the 3D pure phase encoding, which requires longer scan time. The abovementioned WASPI-type approach would allow flexibility to control the central sub-region without fold-over artifact.

The proposed interleaved encoding strategy can be generally combined with various MRI signal preparations utilizing multi-spoke imaging, including fat suppression, magnetization transfer, T1ρ, chemical exchange saturation transfer, and diffusion weighting. For these preparations, the spokes for central region of the k-space, such as SPI or WASPI, can be placed in the front in a group of multi-spokes to better capture the prepared image contrast while it is most effective. Therefore, the key idea of IR-IHE, interleaved encoding, can be broadly used in many other applications besides the myelin imaging.

One limitation in the current *in vivo* myelin imaging protocol is the low spatial resolution (e.g., 1×1×3.6 mm^3 for the *in vivo* protocol). To detect small lesions in the early stages of MS, higher spatial resolution will be required, which will decrease SNR and increase scan time. We will further investigate these issues to optimize the *in vivo* imaging parameters in future studies. In optimization of the imaging parameters, the proposed interleaving scheme will give high flexibility by allowing a high degree of multi-spoking. We will also explore other UTE imaging techniques besides the conventional pure radial UTE and HE, such as ZTE, PETRA, and Cones to improve the direct myelin imaging in terms of SNR, image contrast, spatial resolution, and scan time.

Conclusions

In this study, we demonstrated the efficacy and feasibility of inversion recovery prepared interleaved hybrid encoding for direct qualitative myelin imaging in the human brain, which provides highly specific volumetric myelin images within 7 minutes of scan time.

Supplementary Material

Refer to Web version on PubMed Central for supplementary material.

Acknowledgements

The authors acknowledge grant support from the NIH (1R01 NS092650 and T32 EB005970), VA Clinical Science and Rehabilitation Research and Development Services (Merit Awards I01CX001388 and I01RX002604), and GE Healthcare.

References

1. Vos T, Allen C, Arora M, et al. Global, regional, and national incidence, prevalence, and years lived with disability for 310 diseases and injuries, 1990–2015: a systematic analysis for the Global Burden of Disease Study 2015. Lancet [Internet] 2016;388:1545–1602. doi: 10.1016/S0140-6736(16)31678-6. [PubMed: 27733282]
2. Noseworthy JH, Lucchinetti C, Rodriguez M, Weinshenker BG. Multiple Sclerosis. N. Engl. J. Med [Internet] 2000;343:938–952. doi: 10.1056/NEJM200009283431307. [PubMed: 11006371]
3. Polman CH, Reingold SC, Banwell B, et al. Diagnostic criteria for multiple sclerosis: 2010 Revisions to the McDonald criteria. Ann. Neurol [Internet] 2011;69:292–302. doi: 10.1002/ana.22366. [PubMed: 21387374]
4. Filippi M, Rocca MA. MR Imaging of Multiple Sclerosis. Radiology [Internet] 2011;259:659–681. doi: 10.1148/radiol.11101362. [PubMed: 21602503]
5. Traboulsee A, Simon JH, Stone L, et al. Revised Recommendations of the Consortium of MS Centers Task Force for a Standardized MRI Protocol and Clinical Guidelines for the Diagnosis and Follow-Up of Multiple Sclerosis. Am. J. Neuroradiol [Internet] 2016;37:394–401. doi: 10.3174/ajnr.A4539. [PubMed: 26564433]
6. Alonso-Ortiz E, Levesque IR, Pike GB. MRI-based myelin water imaging: A technical review. Magn. Reson. Med [Internet] 2015;73:70–81. doi: 10.1002/mrm.25198. [PubMed: 24604728]
7. Fan S-J, Ma Y, Chang EY, Bydder GM, Du J. Inversion recovery ultrashort echo time imaging of ultrashort T 2 tissue components in ovine brain at 3 T: a sequential D 2 O exchange study. NMR Biomed [Internet] 2017;30:e3767. doi: 10.1002/nbm.3767.
8. Fan SJ, Ma Y, Zhu Y, Searleman A, Szeverenyi NM, Bydder GM, Du J. Yet more evidence that myelin protons can be directly imaged with UTE sequences on a clinical 3T scanner: Bicomponent T2* analysis of native and deuterated ovine brain specimens. Magn. Reson. Med 2018;80:538–547. doi: 10.1002/mrm.27052. [PubMed: 29271083]
9. Du J, Ma G, Li S, Carl M, Szeverenyi NM, VandenBerg S, Corey-Bloom J, Bydder GM. Ultrashort echo time (UTE) magnetic resonance imaging of the short T2 components in white matter of the brain using a clinical 3T scanner. Neuroimage [Internet] 2014;87:32–41. doi: 10.1016/j.neuroimage.2013.10.053. [PubMed: 24188809]
10. Sheth V, Shao H, Chen J, Vandenberg S, Corey-Bloom J, Bydder GM, Du J. Magnetic resonance imaging of myelin using ultrashort Echo time (UTE) pulse sequences: Phantom, specimen, volunteer and multiple sclerosis patient studies. Neuroimage [Internet] 2016;136:37–44. doi: 10.1016/j.neuroimage.2016.05.012. [PubMed: 27155128]
11. Sheth VR, Fan S, He Q, Ma Y, Annese J, Switzer R, Corey-Bloom J, Bydder GM, Du J. Inversion recovery ultrashort echo time magnetic resonance imaging: A method for simultaneous direct detection of myelin and high signal demonstration of iron deposition in the brain – A feasibility study. Magn. Reson. Imaging [Internet] 2017;38:87–94. doi: 10.1016/j.mri.2016.12.025. [PubMed: 28038965]
12. Waldman A, Rees JH, Brock CS, Robson MD, Gatehouse PD, Bydder GM. MRI of the brain with ultra-short echo-time pulse sequences. Neuroradiology [Internet] 2003;45:887–892. doi: 10.1007/s00234-003-1076-z. [PubMed: 14508620]
13. Horch RA, Gore JC, Does MD. Origins of the ultrashort-T2 1H NMR signals in myelinated nerve: A direct measure of myelin content? Magn. Reson. Med [Internet] 2011;66:24–31. doi: 10.1002/mrm.22980. [PubMed: 21574183]
14. Wilhelm MJ, Ong HH, Wehrli SL, Li C, Tsai P-H, Hackney DB, Wehrli FW. Direct magnetic resonance detection of myelin and prospects for quantitative imaging of myelin density. Proc. Natl. Acad. Sci [Internet] 2012;109:9605–9610. doi: 10.1073/pnas.1115107109. [PubMed: 22628562]
15. Grodzki DM, Jakob PM, Heismann B. Ultrashort echo time imaging using pointwise encoding time reduction with radial acquisition (PETRA). Magn. Reson. Med [Internet] 2012;67:510–518. doi: 10.1002/mrm.23017. [PubMed: 21721039]
16. Emid S, Creyghton JHN. High resolution NMR imaging in solids. Phys. B+C 1985;128:81–83. doi: 10.1016/0378-4363(85)90087-7.

17. Jang H, Wiens CN, McMillan AB. Ramped hybrid encoding for improved ultrashort echo time imaging. Magn. Reson. Med [Internet] 2016;76:814–825. doi: 10.1002/mrm.25977. [PubMed: 26381890]
18. Grodzki DM, Jakob PM, Heismann B. Correcting slice selectivity in hard pulse sequences. J. Magn. Reson [Internet] 2012;214:61–7. doi: 10.1016/j.jmr.2011.10.005. [PubMed: 22047992]
19. Jang H, Liu F, Bradshaw T, McMillan AB. Rapid dual-echo ramped hybrid encoding MR-based attenuation correction (dRHE-MRAC) for PET/MR. Magn. Reson. Med [Internet] 2018;79:2912–2922. doi: 10.1002/mrm.26953. [PubMed: 28971513]
20. Du J, Bydder M, Takahashi AM, Carl M, Chung CB, Bydder GM. Short T2 contrast with three-dimensional ultrashort echo time imaging. Magn. Reson. Imaging [Internet] 2011;29:470–482. doi: 10.1016/j.mri.2010.11.003. [PubMed: 21440400]
21. Chang EY, Du J, Chung CB. UTE imaging in the musculoskeletal system. J. Magn. Reson. Imaging [Internet] 2015;41:870–883. doi: 10.1002/jmri.24713. [PubMed: 25045018]
22. Seifert AC, Li C, Wilhelm MJ, Wehrli SL, Wehrli FW. Towards quantification of myelin by solid-state MRI of the lipid matrix protons. Neuroimage [Internet] 2017;163:358–367. doi: 10.1016/j.neuroimage.2017.09.054. [PubMed: 28964929]
23. Chen J, Carl M, Ma Y, Shao H, Lu X, Chen B, Chang EY, Wu Z, Du J. Fast volumetric imaging of bound and pore water in cortical bone using three-dimensional ultrashort-TE (UTE) and inversion recovery UTE sequences. NMR Biomed [Internet] 2016;29:1373–1380. doi: 10.1002/nbm.3579. [PubMed: 27496335]
24. Chen J, Chang EY, Carl M, Ma Y, Shao H, Chen B, Wu Z, Du J. Measurement of bound and pore water T1 relaxation times in cortical bone using three-dimensional ultrashort echo time cones sequences. Magn. Reson. Med [Internet] 2017;77:2136–2145. doi: 10.1002/mrm.26292. [PubMed: 27263994]
25. Kecskemeti S, Samsonov A, Hurley SA, Dean DC, Field A, Alexander AL. MPnRAGE: A technique to simultaneously acquire hundreds of differently contrasted MPRAGE images with applications to quantitative T1mapping. Magn. Reson. Med 2016;75:1040–1053. doi: 10.1002/mrm.25674. [PubMed: 25885265]
26. Nazaran A, Carl M, Ma Y, Jerban S, Zhu Y, Lu X, Du J, Chang EY. Three-dimensional adiabatic inversion recovery prepared ultrashort echo time cones (3D IR-UTE-Cones) imaging of cortical bone in the hip. Magn. Reson. Imaging [Internet] 2017;44:60–64. doi: 10.1016/j.mri.2017.07.012. [PubMed: 28716680]
27. Jerban S, Ma Y, Wan L, Searleman AC, Jang H, Sah RL, Chang EY, Du J. Collagen proton fraction from ultrashort echo time magnetization transfer (UTE-MT) MRI modelling correlates significantly with cortical bone porosity measured with micro-computed tomography (μCT). NMR Biomed [Internet] 2018;In Press:e4045. doi: 10.1002/nbm.4045. [PubMed: 30549338]
28. Larson PEZ, Conolly SM, Pauly JM, Nishimura DG. Using adiabatic inversion pulses for long-T2 suppression in ultrashort echo time (UTE) imaging. Magn. Reson. Med [Internet] 2007;58:952–961. doi: 10.1002/mrm.21341. [PubMed: 17969119]
29. Jang H, Liu F, Zhao G, Bradshaw T, McMillan AB. Technical Note: Deep learning based MRAC using rapid ultrashort echo time imaging. Med. Phys 2018;45:3697–3704. doi: 10.1002/mp.12964.
30. Blunck Y, Moffat BA, Kolbe SC, Ordidge RJ, Cleary JO, Johnston LA. Zero-gradient-excitation ramped hybrid encoding (zG RF -RHE) sodium MRI. Magn. Reson. Med [Internet] 2019;81:1172–1180. doi: 10.1002/mrm.27484. [PubMed: 30252156]
31. Li C, Magland JF, Zhao X, Seifert AC, Wehrli FW. Selective in vivo bone imaging with long-T2suppressed PETRA MRI. Magn. Reson. Med 2017;77:989–997. doi: 10.1002/mrm.26178. [PubMed: 26914767]
32. Manhard MK, Horch RA, Harkins KD, Gochberg DF, Nyman JS, Does MD. Validation of quantitative bound- and pore-water imaging in cortical bone. Magn. Reson. Med 2014;71:2166–2171. doi: 10.1002/mrm.24870. [PubMed: 23878027]
33. Chan RW, Ramsay EA, Cheung EY, Plewes DB. The influence of radial undersampling schemes on compressed sensing reconstruction in breast MRI. Magn. Reson. Med 2012;67:363–377. doi: 10.1002/mrm.23008. [PubMed: 21656558]

34. Fessler JA. On NUFFT-based gridding for non-Cartesian MRI. J. Magn. Reson 2007;188:191–195. doi: 10.1016/j.jmr.2007.06.012. [PubMed: 17689121]

35. de Lange EE, Mugler JP, Bertolina JA, Gay SB, Janus CL, Brookeman JR. Magnetization Prepared RApid Gradient-Echo (MP-RAGE) MR imaging of the liver: Comparison with spin-echo imaging. Magn. Reson. Imaging [Internet] 1991;9:469–476. doi: 10.1016/0730-725X(91)90031-G. [PubMed: 1779716]

36. Pipe JG, Menon P. Sampling density compensation in MRI: rationale and an iterative numerical solution. Magn. Reson. Med [Internet] 1999;41:179–86. [PubMed: 10025627]

37. Feng L, Grimm R, Block KT, Chandarana H, Kim S, Xu J, Axel L, Sodickson DK, Otazo R. Golden-angle radial sparse parallel MRI: Combination of compressed sensing, parallel imaging, and golden-angle radial sampling for fast and flexible dynamic volumetric MRI. Magn. Reson. Med [Internet] 2014;72:707–717. doi: 10.1002/mrm.24980. [PubMed: 24142845]

38. Chan RW, Ramsay EA, Cunningham CH, Plewes DB. Temporal stability of adaptive 3D radial MRI using multidimensional golden means. Magn. Reson. Med 2009;61:354–363. doi: 10.1002/mrm.21837. [PubMed: 19165897]

39. Wu Y, Dai G, Ackerman JL, Hrovat MI, Glimcher MJ, Snyder BD, Nazarian A, Chesler DA. Water- and fat-suppressed proton projection MRI (WASPI) of rat femur bone. Magn. Reson. Med [Internet] 2007;57:554–567. doi: 10.1002/mrm.21174. [PubMed: 17326184]

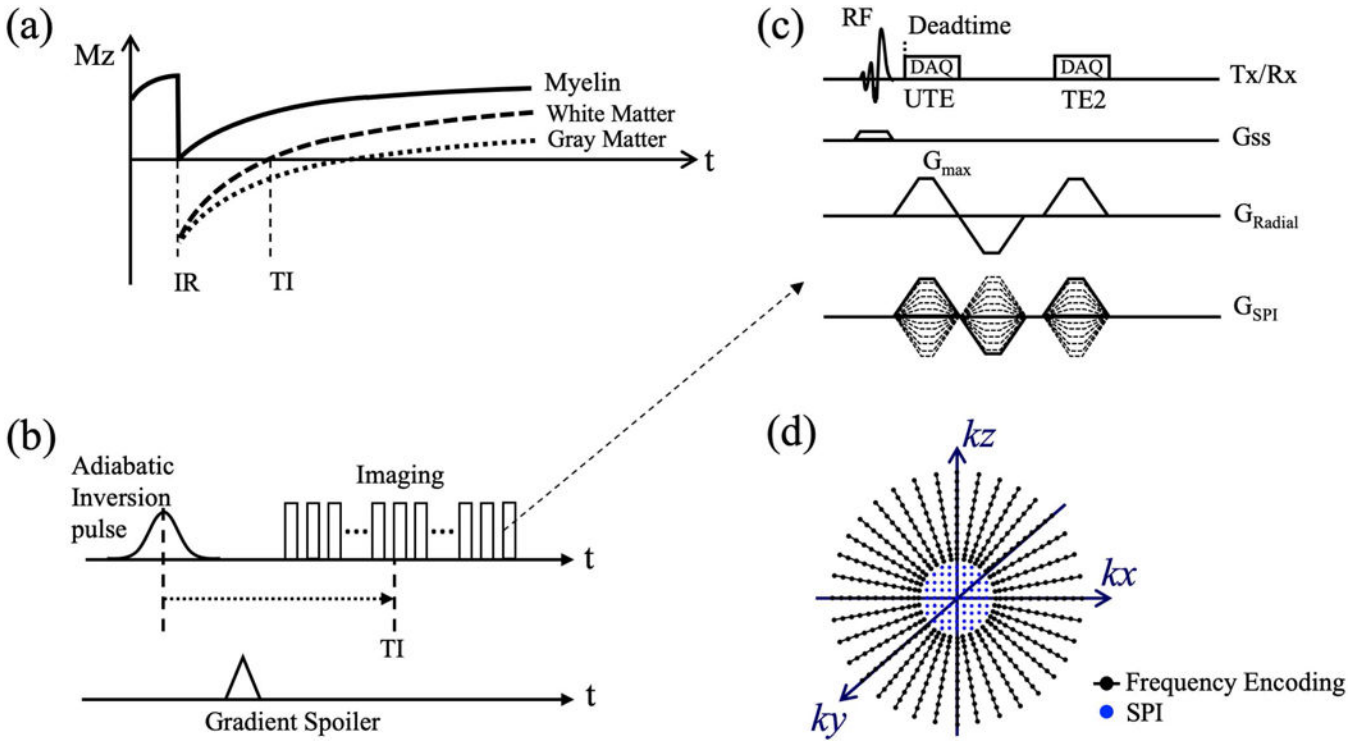

Figure 1.

Inversion recovery prepared hybrid encoding (IR-HE) for direct myelin imaging. (a) Inversion recovery of myelin, white matter, and gray matter; (b) pulse sequence diagram for multi-spoke IR imaging; (c) for dual echo hybrid encoding; and (d) sampling pattern for hybrid encoding. Note that after each IR preparation, multiple spokes are applied centered on the TI to efficiently suppress signals from long T2 white matter, as shown in (b). The remaining signal from gray matter is suppressed by echo subtraction.

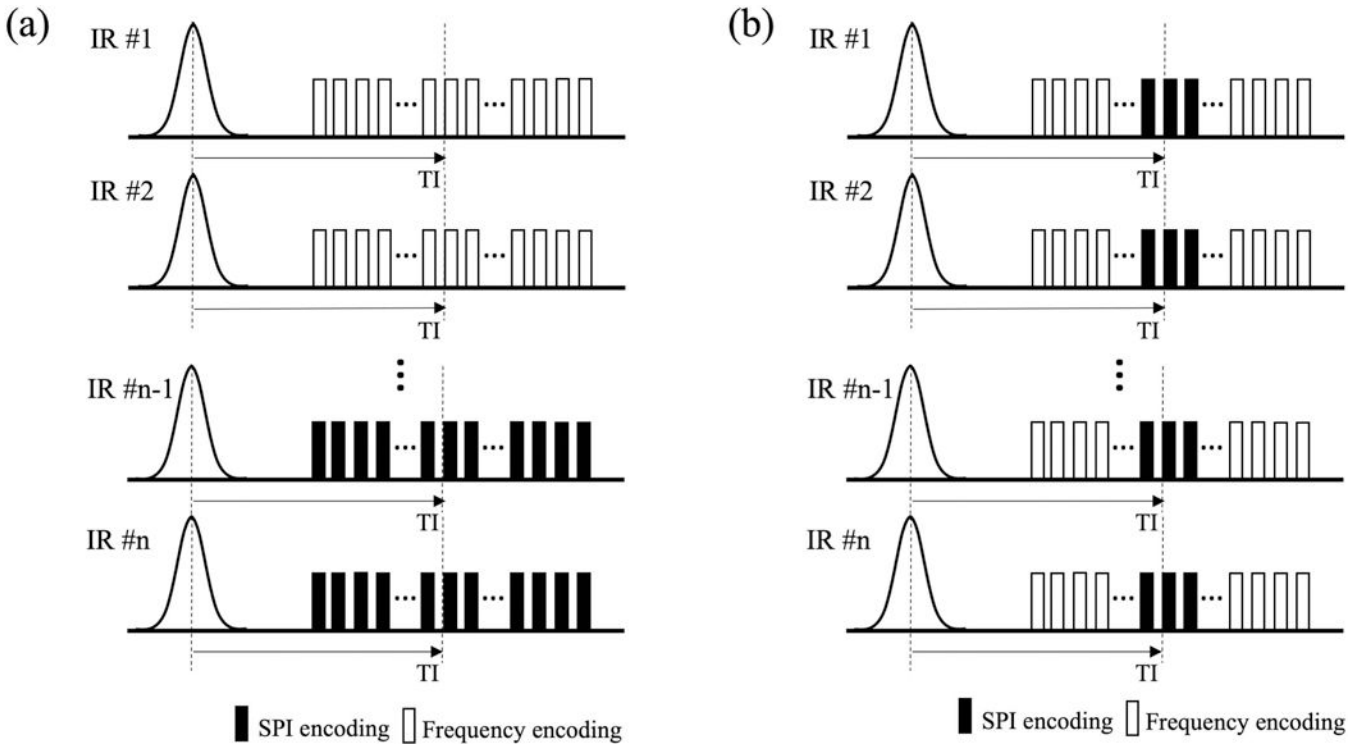

Figure 2.

A new sampling scheme in inversion recovery prepared hybrid encoding (IR-HE). (a) IR-HE with conventional sequential sampling and (b) the proposed IR prepared interleaved hybrid encoding (IR-IHE). In IR-IHE in (b), single point imaging (SPI) encoding is interleaved near the optimal TI (more efficient suppression of signals from long T2 white matter), which can improve myelin image contrast since the central region encoded by SPI contributes most to the image contrast.

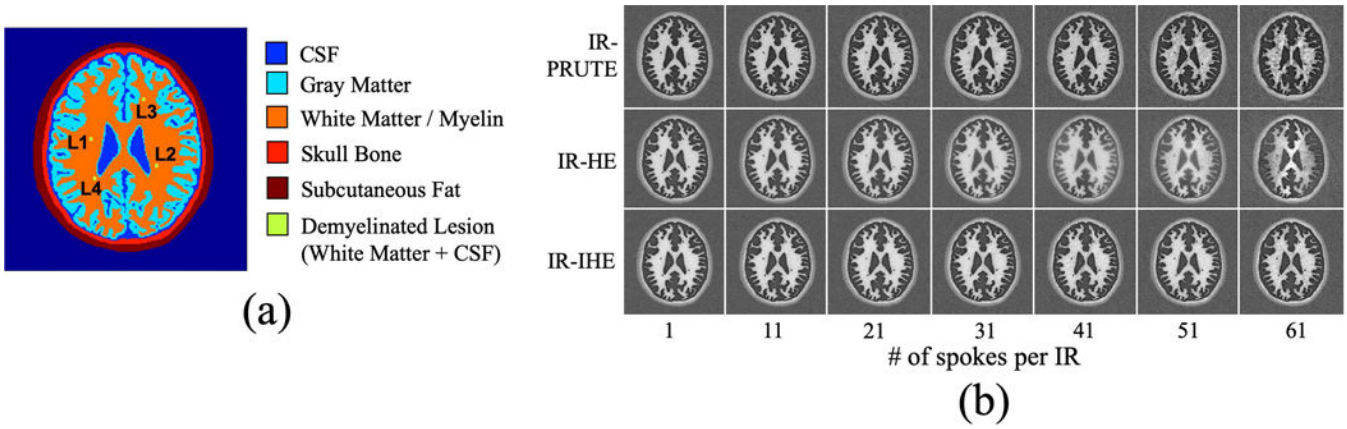

Figure 3.

Computer simulation. (a) Digital phantom design, which includes 6 major components of the human brain (myelin, white matter, gray matter, skull bone, subcutaneous fat, and CSF) and (b) simulated myelin images with inversion recovery prepared pure radial UTE (IR-PRUTE), IR prepared hybrid encoding (IR-HE), or IR prepared interleaved hybrid encoding (IR-IHE). Different numbers of spokes per IR were individually simulated. Note that in (b), with higher number of multi-spokes per IR, IR-PRUTE exhibits worsened image quality with streaking artifact, while IR-HE shows low-frequency signal bias. More results can be found in Supporting Information Figure S1, and the results with the expanded simulations with different Taus and myelin densities can be found in Supporting Information Figure S2 and S3, respectively.

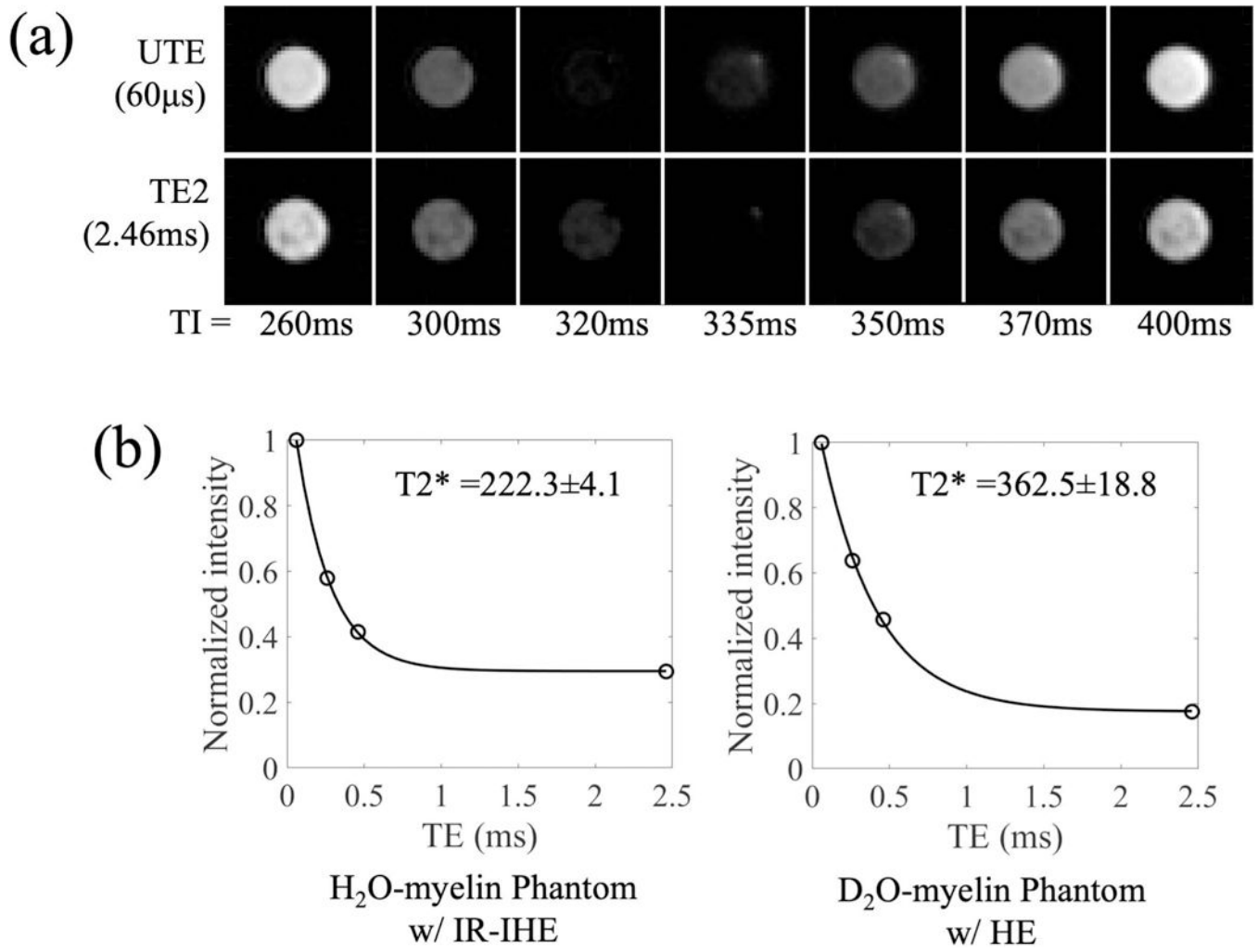

Figure 4.

Myelin phantom experiment. (a) H_2O-myelin phantom images acquired with interleaved hybrid encoding (IR-IHE at TE = 0.06 ms or 2.46 ms at different TIs ranging from 260 to 400 ms), and (b) T2* fitting in H_2O-myelin phantom and D_2O-myelin phantom. The phantoms were prepared using bovine-extracted myelin lipid powder at 15% weight/volume (w/v). The best TI of 335 ms found from the experiment in (a) was then used in the T2* fitting in (b). D_2O-myelin phantom was imaged with HE-UTE without IR preparation. The slightly elevated T2* was observed in the D_2O-myelin phantom experiment in (b), presumably due to residual contaminating H_2O.

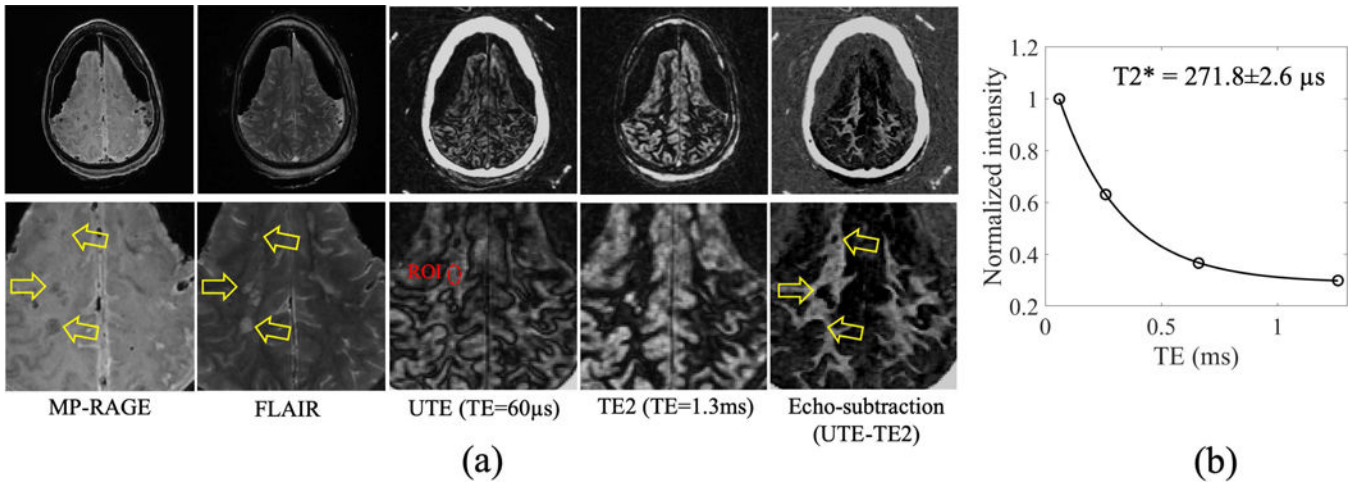

Figure 5.

Inversion recovery prepared interleaved hybrid encoding (IR-IHE) images of a cadaveric MS brain from a 45-year-old male donor. (a) Clinical images (MP-RAGE and FLAIR) and the IR-IHE (UTE, TE2, and the echo subtraction) and (b) T2* fitting in IR-IHE. Demyelinated lesions can be clearly seen in the difference image. T2* estimated in the ROI in (a) was 271.8±2.6 μs, which is close to the T2* of myelin in H_2O-myelin or D_2O-myelin phantom in Figure 4, as well as the T2* reported in the literature (~150–400 μs).

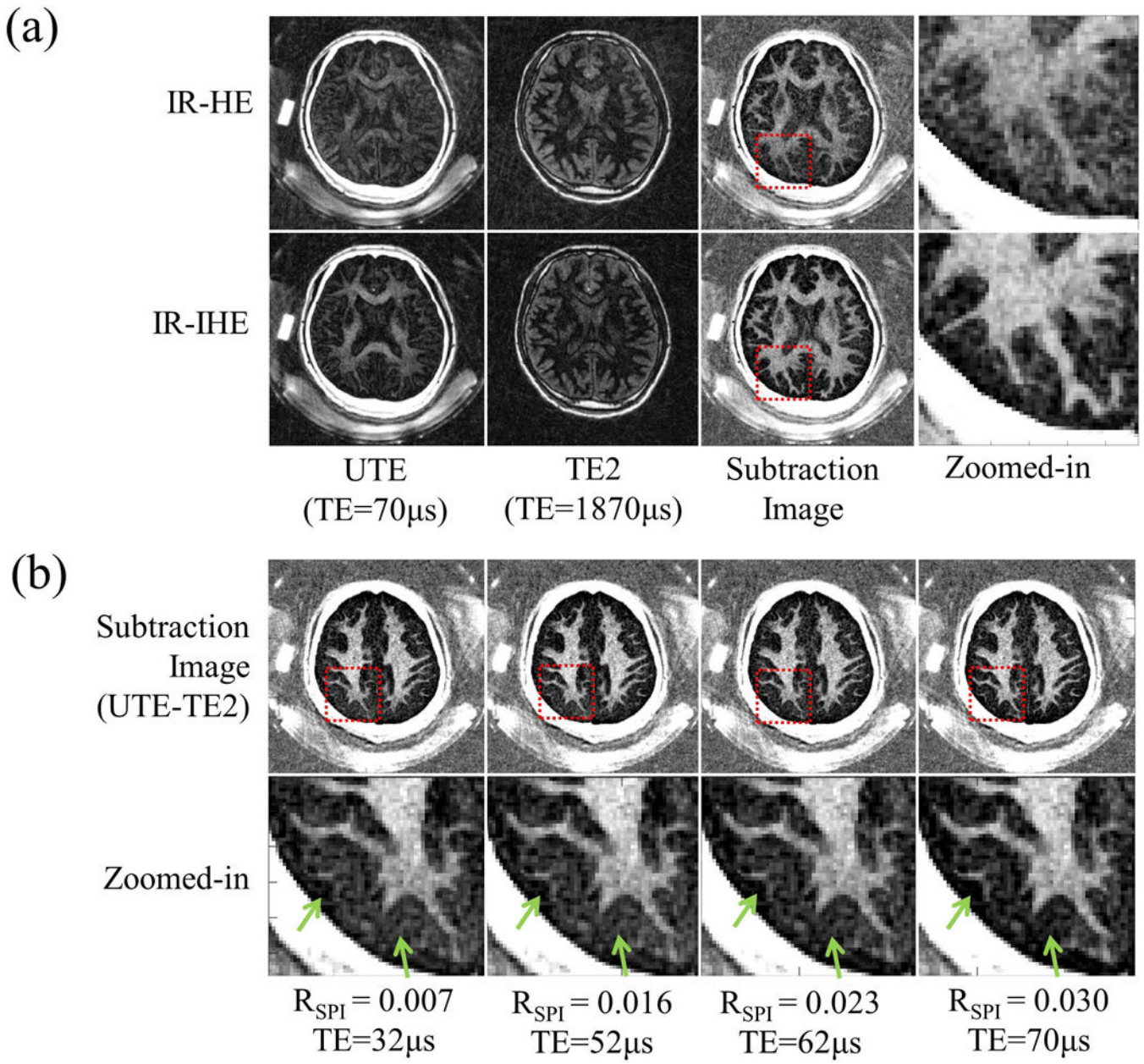

Figure 6.

Myelin imaging of a 30-year-old healthy male volunteer obtained using the inversion recovery prepared hybrid encoding (IR-HE) or IR prepared interleaved hybrid encoding (IR-IHE). (a) Efficacy of IR-IHE and (b) myelin image contrasts with different sizes of k-space subregion encoded by single point imaging (SPI) in the IR-IHE. The R_{SPI} was defined by the ratio of the maximum k-space coordinate in SPI to the maximum coordinate in entire k-space. In (a), IR-IHE dramatically improved the contrast of the myelin image, where the measured contrast-to-noise ratio (CNR) between myelin and the surrounding tissues was 2.3±0.6 in the IR-HE and 4.8±0.7 in the IR-IHE. The images with the larger SPI exhibit improved myelin contrast as indicated by the green arrows in (b). The measured CNR

between myelin and the surrounding tissues was 3.5±0.8, 3.9±0.7, 4.1±0.7, and 4.8±0.7, respectively, with R_{SPI} = 0.007, 0.016, 0.023, and 0.030.

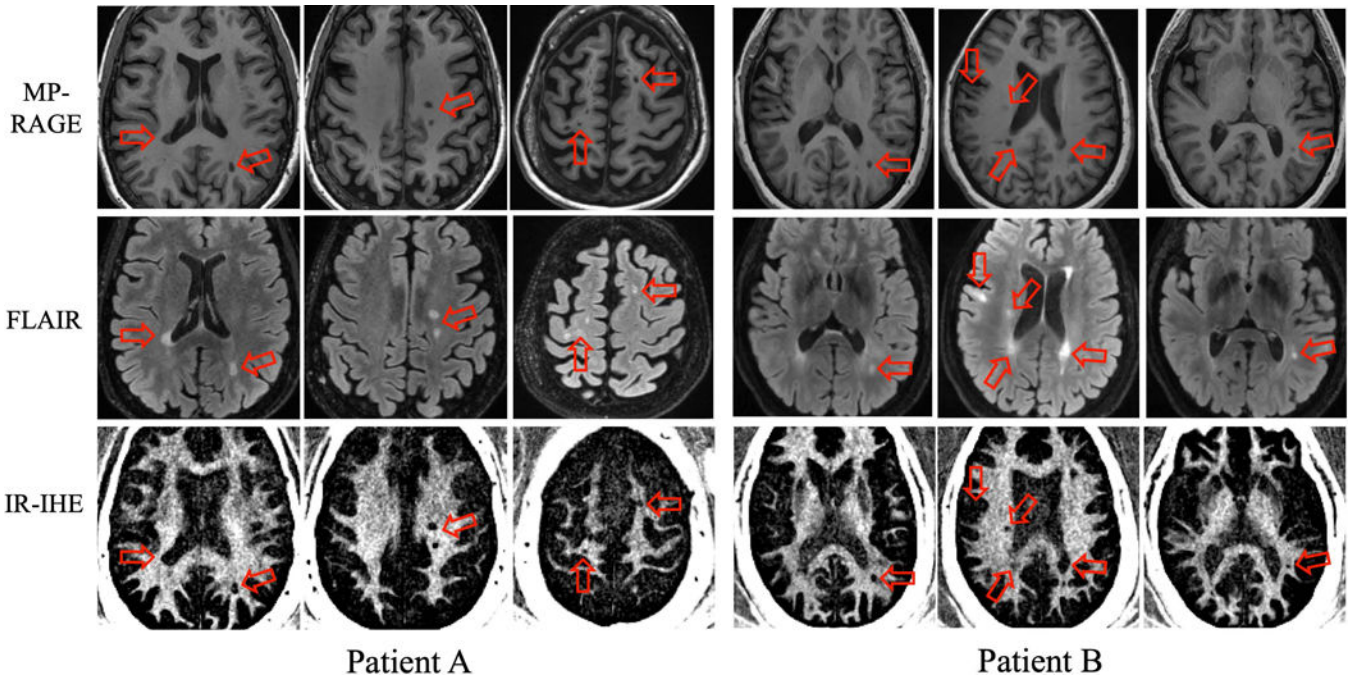

Figure 7.

Imaging of two representative MS patients (Patient A: 59-year-old female, Patient B: 51-year-old female) with the inversion recovery prepared interleaved hybrid encoding (IR-IHE) compared with CSF-suppressed T1-weighted MP-RAGE and T2-weighted FLAIR sequences. As indicated by red arrows, IR-IHE can directly detect the demyelinated areas, thus providing more direct and specific morphological information of the lesions compared with the clinical sequences.